Illuminating the Surface Spin Texture of the Giant-Rashba Quantum-Well System Bi/Ag(111) by Circularly Polarized Photoemission

Guang Bian, Longxiang Zhang, Yang Liu, T. Miller, and T.-C. Chiang

Department of Physics, University of Illinois at Urbana-Champaign, 1110 West Green Street, Urbana, Illinois 61801-3080, USA
Frederick Seitz Materials Research Laboratory, University of Illinois at Urbana-Champaign, 104 South Goodwin Avenue, Urbana, Illinois 61801-2902, USA

(Received 2 February 2012; published 2 May 2012)

We have mapped out the spin texture of a Bi/Ag surface alloy prepared on a thin Ag film by circularly polarized angle-resolved photoemission spectroscopy. A term proportional to $\nabla \cdot \mathbf{A}$ in the interaction Hamiltonian gives rise to strong surface photoexcitation, which interferes with a Rashba contribution to yield a pronounced circular dichroic effect in Bi/Ag. The dipole transition, often taken to be the only important photoexcitation mechanism, is actually negligible. A parameter-free calculation yields a dichroic pattern in excellent agreement with experiment.

DOI: 10.1103/PhysRevLett.108.186403 PACS numbers: 71.70.Ej, 73.20.At, 79.60.Dp

One-third of a monolayer (ML) of Bi alloyed into a Ag(111) surface yields a free-electron-like surface state with the largest known Rashba spin splitting [1,2], a property of great interest in connection with the search for exotic phases including two-dimensional superconductors and Majorana states [3]. We show how the complex spin texture [4,5] resulting from the entanglement of this surface state with the quantum-well states in a thin Ag(111)-film substrate can be unraveled by circularly polarized angle-resolved photoemission spectroscopy (CARPES). CARPES has emerged as a powerful method for probing spin, pseudospin, and correlated electron structures [6–9], but a comprehensive theoretical basis has been lacking. We show that the strong dichroic pattern in Bi/Ag arises from the interference between two surface photoemission contributions, the Rashba interaction [7], and an often-neglected nonzero $\nabla \cdot \mathbf{A}$ [10–12], as demonstrated by excellent agreement between a parameter-free calculation and experiment.

The giant Rashba spin splitting in surface alloys is also of great interest for spintronic applications, but the metallic substrate can act as an electrical short and a source of scattering. Surface alloys based on ultrathin films are much more promising for applications, as the reduced bulk part of the system limits the number of bulk conduction channels near the Fermi level, resulting in an enhanced surface contribution to the net system response. Ultrathin films are furthermore amenable to gate tuning. We have chosen to focus on Bi deposited on nanometer-scale Ag(111) films as a prototypical system. Ag films of atomic layer uniformity can be readily grown on Si(111), the most common semiconductor substrate material. The quantization of the electronic states in the film results in discrete quantum-well states that can be adjusted by varying the film thickness [13,14]. The entanglement of the alloy surface state and the quantum-well states leads to a complex surface spin texture in Bi/Ag, which is an ideal test ground for the basic physics of dichroism based on CARPES in terms of electromagnetic interactions with surface charge and spin. The method should be of general utility for probing novel states of matter.

The sample configuration and lattice structure of Bi/Ag(111) are indicated in Figs. 1(a)–1(c). The 1/3 ML of Bi organizes into a $\sqrt{3} \times \sqrt{3}$ structure in the top atomic layer. For comparison, we also examine a similar surface alloy system Sb/Ag(111), which exhibits a much smaller spin splitting. The Bi and Sb atoms are located higher than the top Ag atomic plane by $d = 0.65$ and 0.10 Å, respectively [15]. The surface Brillouin zones of the surface alloy and the Ag(111) film are shown in Fig. 1(d); they are related by a 30° rotation and a length ratio of $\sqrt{3}$. We use the labels $\bar{\Gamma}$, $\bar{M}$, and $\bar{K}$ for the special points in the Brillouin zone of the $\sqrt{3} \times \sqrt{3}$ surface alloy, and the corresponding primed quantities for the Ag film surface.

A typical photoemission spectral map taken from Bi/Ag prepared on a 20 ML Ag film is presented in Fig. 1(e). The map is taken along $\bar{M}$-$\bar{\Gamma}$-$\bar{M}$ and reaches the $\bar{\Gamma}$ point of the second Brillouin zone of the surface alloy, which coincides with the $\bar{K}'$ point of the first Brillouin zone of the Ag(111) film. The pair of intense concave parabolic bands symmetric about the first $\bar{\Gamma}$ point is the Bi-induced surface states with the characteristic Rashba splitting [16]. In the background centered around $\bar{\Gamma}$ is a set of convex parabolic subbands associated with the quantum-well states in the Ag film. They become more densely packed as the Ag(111) film thickness increases, while the surface state bands remain unchanged. Anticrossing or hybridization gaps arise where the surface bands cross the quantum-well subbands [17,18], giving rise to the strong modulations of the surface band intensities. Similar patterns are seen around the second $\bar{\Gamma}$ point, where umklapp scattering by the $\sqrt{3} \times \sqrt{3}$ reconstructed surface potential yields the weaker replica emission from the quantum-well subbands [19].

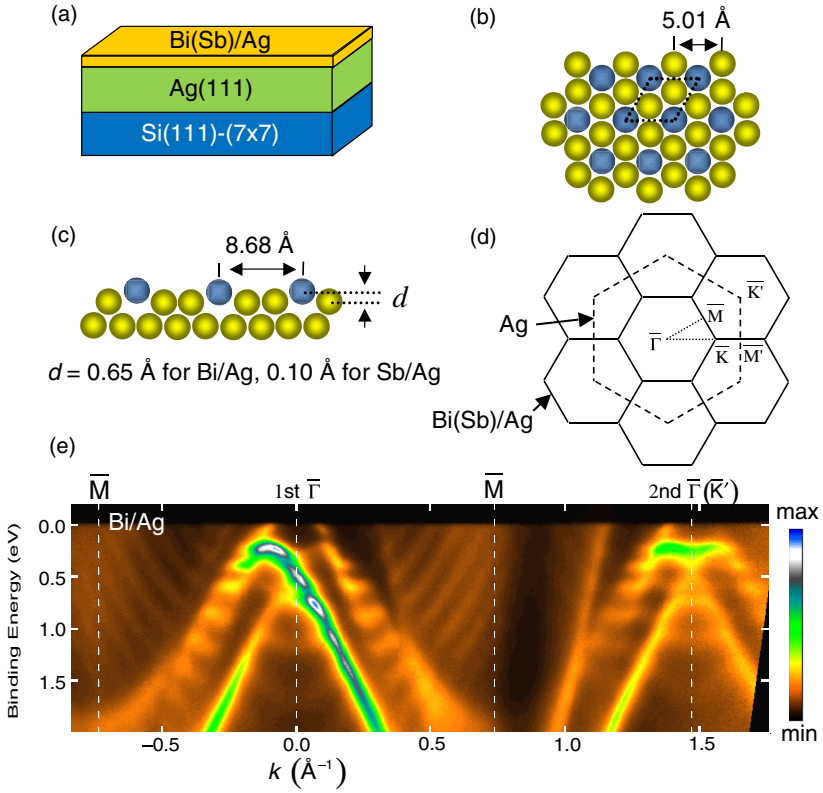

FIG. 1 (color online). Structures of Bi(Sb)/Ag surface alloys and photoemission data from Bi/Ag. (a) Sample configuration. (b) and (c) Top and side views of the lattice structures of the surface alloys. Blue balls indicate Bi or Sb atoms and yellow balls stand for silver atoms. (d) Surface Brillouin zones of the surface alloy and Ag(111) films. $\overline{\Gamma M} = 0.73$ Å^{-1} and $\overline{\Gamma K} = 0.84$ Å^{-1}. (e) Photoemission map taken from Bi/Ag based on a 20-ML Ag film. The spectrum is mapped along $\bar{M}$-$\bar{\Gamma}$-$\bar{M}$ using 22 eV horizontally polarized photons.

The experimental geometry is present in Fig. 2(a). We take the normal of the sample to be along $\hat{\mathbf{z}}$ and the $\overline{\Gamma M}$ direction to be along $\hat{\mathbf{x}}$. The incident photon beam is in the xz plane at an angle of $\theta \approx 60°$. The polarization vector of vertically polarized (VP) light is along $\hat{\mathbf{y}}$, and that of the horizontally polarized (HP) light lies within the xz plane; here, "vertical" and "horizontal" refer to the plane of the electron storage ring used as the photon source. A schematic band diagram for the surface alloy (without the underlying quantum-well states), assuming a large spin splitting appropriate for Bi/Ag, is presented in Fig. 2(b) with red and blue colors indicating opposite Rashba spin directions $\pm\boldsymbol{k} \times \hat{\mathbf{z}}$. For Sb/Ag, the red and blue bands in each pair nearly coincide and cannot be resolved experimentally. Spectra of Sb/Ag prepared on a 22-ML Ag(111) film taken along $\bar{K}$-$\bar{\Gamma}$-$\bar{K}$ and $\bar{M}$-$\bar{\Gamma}$-$\bar{M}$ with HP light are shown in Figs. 2(c) and 2(d), respectively. The intense concave surface band at binding energies larger than 0.4 eV originates from the Sb s-p_z orbitals. The other weaker surface band poking through the Fermi level is derived from the Sb p_x-p_y orbitals [20,21]. The underlying quantum-well subbands are weak but evident. The corresponding spectrum taken along $\bar{M}$-$\bar{\Gamma}$-$\bar{M}$ from Bi/Ag prepared on a 20-ML Ag(111) film [Fig. 2(e)] shows a large Rashba splitting. Since the p_x-p_y bands have weak intensities, especially along the $\bar{\Gamma}$-$\bar{M}$ direction, we shall focus on the s-p_z bands only.

The Rashba-split s-p_z bands can be described by the dispersion relations

$$E(k) = E_0 - \frac{(k \pm k_0)^2}{2m^*}, \tag{1}$$

where m^* is the effective mass of each holelike band. The momentum offset k_0 is determined by the strength of the Rashba interaction and equals 0.005 Å^{-1} for Sb/Ag and 0.13 Å^{-1} for Bi/Ag; the latter is much larger partly because of the larger atomic mass of Bi but mostly because of the larger outward relaxation d of the Bi atoms relative to the surface Ag atomic plane resulting in a stronger surface potential gradient. The two spin-split s-p_z bands in Bi/Ag show very different intensities in Fig. 2(e), implying a strong spin-dependent photoemission process.

Photoemission is governed by the interaction Hamiltonian

$$\Delta H \propto \mathbf{A} \cdot \nabla + \tfrac{1}{2}\nabla \cdot \mathbf{A} + \alpha \mathbf{s} \cdot \mathbf{A} \times \nabla V, \tag{2}$$

where $\mathbf{A}$ is the vector potential of the incident light. The first term corresponds to dipole transition and is the dominant contribution for bulk direct transitions governed by momentum conservation in all three dimensions. It is

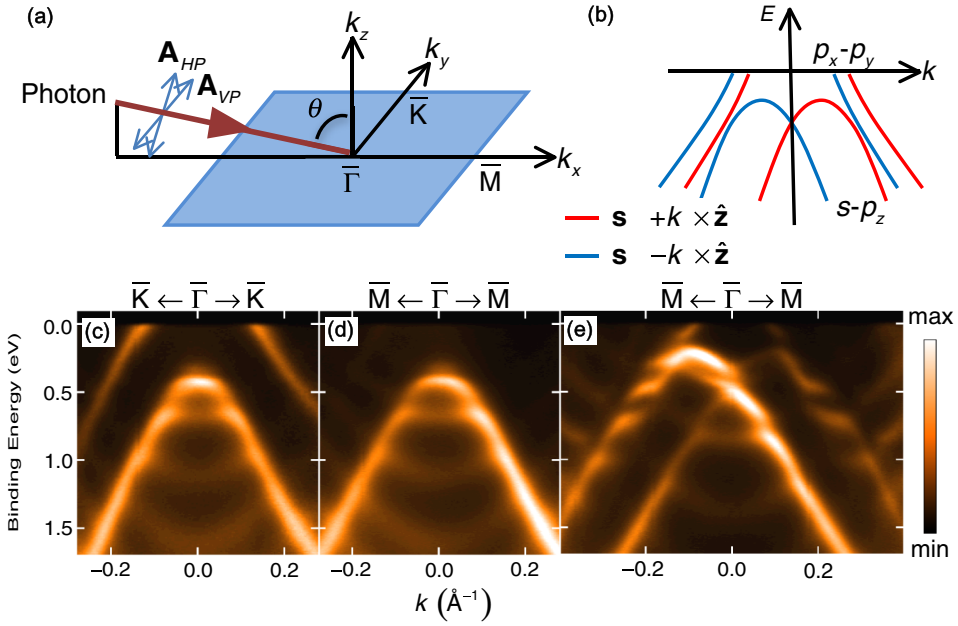

FIG. 2 (color online). Experimental geometry and ARPES maps from Bi(Sb)/Ag(111) surface alloys taken with HP light at 22 eV. (a) Experimental geometry. The normal of the sample surface is along $\hat{\mathbf{z}}$ and the vertical direction is along $\hat{\mathbf{y}}$ in the laboratory frame of reference. (b) Schematic band dispersion relations and spin textures of Bi/Ag; Sb/Ag has similar band dispersion relations but the spin splittings are much smaller and not apparent in the data. (c) and (d) Photoemission results taken along $\bar{K}$-$\bar{\Gamma}$-$\bar{K}$ and $\bar{M}$-$\bar{\Gamma}$-$\bar{M}$ directions, respectively, from Sb/Ag based on a 22-ML Ag film. (e) Photoemission results taken along $\bar{M}$-$\bar{\Gamma}$-$\bar{M}$ from Bi/Ag based on a 20-ML Ag film.

generally negligible for surface and quantum-well states away from direct transitions. The second term, known as the surface-photoemission term, is important only at the surface where the dielectric function ε and hence the vector potential $\mathbf{A}$ are discontinuous [10–12]. The discontinuity results in a $\nabla \cdot \mathbf{A}$ peaked around the surface. The third term depends on the spin $\mathbf{s}$ explicitly and stems from the Rashba interaction [7], where the canonical momentum depends on $\mathbf{A}$. It also peaks around the surface because of the gradient of the surface potential ∇V.

With the first term in Eq. (2) ignored [14], the photoemission matrix element becomes

$$\langle \Psi_f | \Delta H | \Psi_i \rangle \propto \left[\frac{\hbar e}{2m_e} \left(1 - \frac{1}{\varepsilon}\right) A_z + \frac{d\beta e}{\hbar} \mathbf{A} \times \boldsymbol{\sigma} \cdot \hat{\mathbf{z}} \right] \Psi_f^*(0) \Psi_i(0), \quad (3)$$

where $\Psi_f^*(0)\Psi_i(0)$ is the product of the initial and final state wave functions at the surface, $\varepsilon = 1.26 + 2.03i$ for Ag at 22 eV [22], $d = 0.65$ Å is the outward relaxation of the Bi atoms, $\boldsymbol{\sigma}$ is the normalized spin polarization of the initial state, and the Rashba parameter $\beta = 3.05$ eV-Å is determined from the measured k_0. The product $\Psi_f^*(0)\Psi_i(0)$ is a smooth function of energy and momentum and is taken to be a constant in our calculation over the limited data range. Thus, apart from an overall proportional constant, Eq. (3) contains no arbitrary or unknown parameters. To calculate the photoemission spectral map, we set up a Hamiltonian containing the spin-split bands [Eq. (1)] and a set of parabolic quantum-well subbands positioned to correspond to the experiment. A spin-independent coupling term is included to generate the anticrossing gaps as seen in the experiment. Diagonalization of the Hamiltonian yields $\boldsymbol{\sigma}$, from which the photoemission spectral maps are computed for various polarization configurations including HP, VP, left circular polarization (LCP), and right circular polarization (RCP) by taking the absolute square of the matrix element. Here, "left" and "right" refer to an observer viewing along the incident beam at the sample. A small constant lifetime broadening is included in the calculation.

Data taken along $\bar{M}$-$\bar{\Gamma}$-$\bar{M}$ at 22 eV with HP, LCP, and RCP from Bi/Ag based on a 20-ML Ag film are presented in Figs. 3(a)–3(c). The calculated band dispersions [Fig. 3(d)] show the surface bands, the quantum-well bands, and the anticrossing gaps. Remaining in the gaps are the quantum-well states with the opposite spin orientation than the crossing surface bands. With k_x pointing along $\bar{\Gamma}$-$\bar{M}$, the only nonzero spin component is σ_y. The xz plane, which contains the incident photon beam, is a mirror plane of the sample. As a result of the overall symmetry of the system, LCP is equivalent to RCP, and there should not be any circular dichroism. Indeed, the LCP and RCP data appear to be identical, and the surface band with spin polarization along $+\hat{\mathbf{y}}$ is much more intense than the other surface band with spin polarization along $-\hat{\mathbf{y}}$. The same intensity imbalance is evident in the HP data. A calculated photoemission map [Fig. 3(e)] for

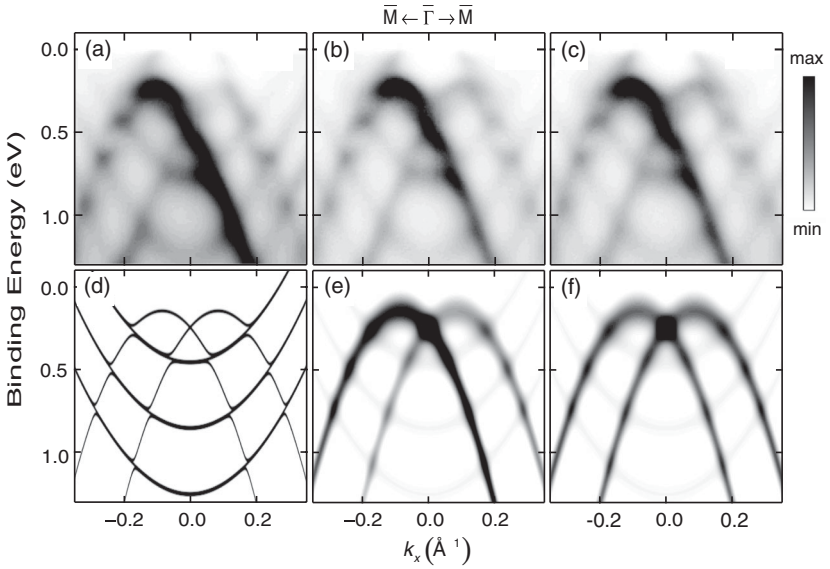

FIG. 3. Photoemission results taken from Bi/Ag based on a 20-ML Ag film. The data were taken along $\bar{M}$-$\bar{\Gamma}$-$\bar{M}$ using 22-eV photons and (a) HP, (b) LCP, and (c) RCP polarization configurations. (d) Calculated band structure showing the hybridization of s-p_z surface bands with quantum-well bands of the Ag film. (e) Calculated photoemission map for HP. (f) Calculated photoemission map for HP assuming that the spin-orbit-coupling contribution to surface photoemission is zero.

HP shows indeed an intensity imbalance in agreement with the data. By contrast, the same calculation, assuming no spin-orbit coupling by setting β to zero, yields a map with equal intensities for the two bands [Fig. 3(f)]. The results indicate that the intensity imbalance between the two bands is a spin effect, despite the lack of circular dichroism.

Circular dichroism becomes apparent for measurements along $\bar{K}$-$\bar{\Gamma}$-$\bar{K}$, for which the system no longer possesses mirror symmetry about the xz plane. While the HP map [Fig. 4(a)] shows equal intensities for the two spin-split bands, the LCP and RCP maps [Figs. 4(b) and 4(c)] show different intensities. In fact, the LCP and RCP maps appear to be left-right mirror images of each other about $\bar{\Gamma}$. To quantify this difference, we define a dichroic function

$$\xi = \frac{I_L - I_R}{I_L + I_R}, \tag{4}$$

where $I_{L,R}$ are the photoemission intensities for LCP and RCP, respectively. The experimental results are presented in Fig. 4(d), where red and blue colors indicate positive and negative values of ξ, respectively. The maximum value of ξ is about $\pm 30\%$ at the top of each surface band and the sign of ξ is opposite for the two bands. Figure 4(e) shows the theoretical spin polarization inherited from the Rashba split surface states. States with spin polarization along $+\hat{\mathbf{x}}$ and $-\hat{\mathbf{x}}$ directions are colored in red and blue, respectively. Near the hybridization gaps, the states transform smoothly from surfacelike to bulklike and the hybrid states are partially spin polarized. The calculated dichroic function [Fig. 4(f)] is in excellent agreement with the experimental pattern. The maximum value of ξ is $\pm 38.9\%$ from the

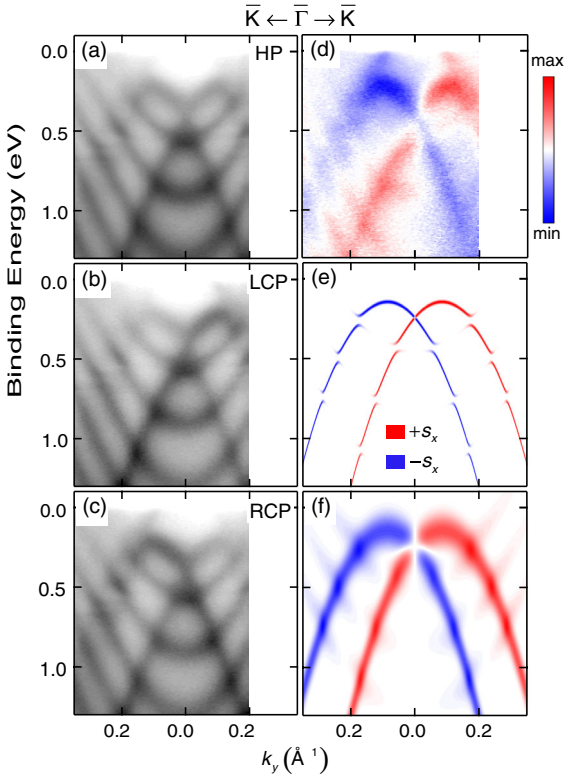

FIG. 4 (color online). Photoemission results taken from Bi/Ag based on a 20 ML Ag film. The data were taken along $\bar{K}$-$\bar{\Gamma}$-$\bar{K}$ using 22-eV photons and (a) HP, (b) LCP, and (c) RCP polarization configurations. (d) Dichroic function extracted from the data. (e) Calculated band structure weighted by the spin polarization inherited from the Rashba split surface states using red and blue colors. (f) Calculated dichroic function.

calculation. It is somewhat higher than the experimental value; the difference can be attributed to the less than perfect polarization state of the LCP and RCP light [14] and possibly to sample imperfections.

The good agreement between experiment and our calculation under various experimental conditions is a strong testimony of the theoretical treatment. The results confirm the strong spin texture of Bi/Ag including the complex pattern of interference between the spin-polarized surface states and the unpolarized quantum-well states. A key finding is that the surface-photoemission term derived from a nonzero $\nabla \cdot \mathbf{A}$ and the $\mathbf{A}$-dependent part of the Rashba interaction can interfere with each other and are both important for understanding our results. The $\nabla \cdot \mathbf{A}$ term has been largely ignored in prior publications, and our analysis here is the first quantitative study of spin-orbit coupling effects taking both terms into account. The methodology developed here should be valuable for unraveling the electronic structure of complex systems including topological insulators, heavy-element compounds, superconductors, and strongly correlated systems in general [23–26].

This work is supported by the U.S. Department of Energy (Grant No. DE-FG02-07ER46383). The Synchrotron Radiation Center, where the ARPES data were taken, is supported by the U.S. National Science Foundation (Grant No. DMR-05-37588). We acknowledge the ACS Petroleum Research Fund and the U.S. National Science Foundation (Grant No. DMR-09-06444) for partial support of beamline operations.

[1] C. Ast *et al.*, Phys. Rev. Lett. **98**, 186807 (2007).
[2] H. Bentmann *et al.*, Europhys. Lett. **87**, 37003 (2009).
[3] A. C. Potter and P. A. Lee, Phys. Rev. Lett. **105**, 227003 (2010).
[4] K. He *et al.*, Phys. Rev. Lett. **104**, 156805 (2010).
[5] F. Meier, H. Dil, J. Lobo-Checa, L. Patthey, and J. Osterwalder, Phys. Rev. B **77**, 165431 (2008).
[6] V. B. Zabolotnyy *et al.*, Phys. Rev. B **76**, 024502 (2007).
[7] Y. H. Wang *et al.*, Phys. Rev. Lett. **107**, 207602 (2011).
[8] Y. Liu, G. Bian, T. Miller, and T. C. Chiang, Phys. Rev. Lett. **107**, 166803 (2011).
[9] Y. Ishida *et al.*, Phys. Rev. Lett. **107**, 077601 (2011).
[10] T. Miller, W. E. McMahon, and T.-C. Chiang, Phys. Rev. Lett. **77**, 1167 (1996).
[11] T. Miller, E. D. Hansen, W. E. McMahon, and T.-C. Chiang, Surf. Sci. **376**, 32 (1997).
[12] E. D. Hansen, T. Miller, and T.-C. Chiang, Phys. Rev. Lett. **78**, 2807 (1997).
[13] T.-C. Chiang, Surf. Sci. Rep. **39**, 181 (2000).
[14] See supplemental material at http://link.aps.org/supplemental/10.1103/PhysRevLett.108.186403.
[15] I. Gierz *et al.*, Phys. Rev. B **81**, 245430 (2010).
[16] Y. A. Bychkov and E. I. Rashba, J. Phys. C **17**, 6039 (1984).
[17] E. Frantzeskakis *et al.*, Phys. Rev. Lett. **101**, 196805 (2008).
[18] K. He *et al.*, Phys. Rev. Lett. **101**, 107604 (2008).
[19] S.-J. Tang, Y. R. Lee, S. L. Chang, T. Miller, and T. C. Chiang, Phys. Rev. Lett. **96**, 216803 (2006).
[20] L. Moreschini *et al.*, Phys. Rev. B **79**, 075424 (2009).
[21] G. Bihlmayer, S. Blügel, and E. V. Chulkov, Phys. Rev. B **75**, 195414 (2007).
[22] H. J. Hagemann, W. Gudat, and C. Kunz, J. Opt. Soc. Am. **65**, 742 (1975).
[23] M. Z. Hasan and C. L. Kane, Rev. Mod. Phys. **82**, 3045 (2010).
[24] X.-L. Qi and S.-C. Zhang, Rev. Mod. Phys. **83**, 1057 (2011).
[25] I. Gierz *et al.*, Phys. Rev. Lett. **103**, 046803 (2009).
[26] K. Yaji *et al.*, Nature Commun. **1**, 1 (2010).